Vortex lattices in layered superconductors

Vesna Prokić
Department of Physics, University of Belgrade, P.O. Box 368, 11001 Belgrade, Yugoslavia

Dragomir Davidović
Department of Physics and Astronomy, The Johns Hopkins University, Bloomberg Center, Baltimore, Maryland 21218 and Institute of Physics, P.O. Box 57, 11001 Belgrade, Yugoslavia

Ljiljana Dobrosavljević-Grujić
Institute of Physics, P.O. Box 57, 11001 Belgrade, Yugoslavia
(Received 14 October 1993; revised manuscript received 7 February 1994)

We study vortex lattices in a superconductor–normal-metal superlattice in a parallel magnetic field. Distorted lattices, resulting from the shear deformations along the layers, are found to be unstable. Under field variation, nonequilibrium configurations undergo an infinite sequence of continuous transitions, typical for soft lattices. The equilibrium vortex arrangement is always a lattice of isocell triangles, without shear.

I. INTRODUCTION

Since the discovery of the high-temperature superconductors (HTS), interest in studying the vortex configurations in layered superconductors has been greatly increased. Recently, shear instabilities of vortex lattices in a low magnetic field parallel to the layers have been predicted. It was shown that the formation of new lattices, obtained by shear deformations, corresponds to bifurcation points labeled by pairs of two consecutive Fibonacci numbers.[1,2] A Fibonacci-type order was observed for the first time in botany. The arrangement of leaves or seeds in plants in the form of regular lattices formed by quantized spirals is known as phyllotaxis. The numbers of spirals, left hand and right hand, are always consecutive terms (F_{N-1},F_N) in the Fibonacci series $F_N=1,1,2,3,5,8,\ldots$. This is related to the fact that the divergence ϕ_d, defined as the angle between the radial directions of the sites $N-1$ and N, is always very close to the golden section, $2\pi(1-\tau)$, and that the ratio F_{N-1}/F_N tends to the golden number $\tau=(\sqrt{5}-1)/2$ in the limit of large N.[3] Similar phyllotaxsislike patterns have been obtained in a physical experiment with ferrofluid drops, and in a numerical simulation of the dynamics of particles interacting via several types of repulsive potentials.[4] All these results show, as pointed out in Ref. 1, that phyllotaxis is a general phenomenon that occurs in all soft lattices subjected to strong deformations.

In Refs. 1 and 2, phyllotaxis structures in commensurate (C) vortex lattices were considered. In both cases, the energy gain due to the pinning induced by the periodic distribution of layers was assumed to be greater than the energy of the elastic deformation needed to achieve the commensurability.[1] Such configurations may occur in a HTS, due to strong intrinsic pinning,[5] particularly at low fields, since the shear modulus of deformation along the hard direction perpendicular to the layers vanishes as $H\rightarrow H_{c1}$,[6] so that the vortices cannot cross the layers. In the above studies,[1,2] the pinning strength is invoked only to set up the model, and the shear deformations are assumed to occur in the easy direction (along the layers). The energies of distorted C lattices are calculated within the London theory for spatially uniform anisotropic superconductors.

The aim of the present work is to study the vortex arrangement in a layered superconductor, taking explicitly into account the discrete structure and the vortex interaction with inhomogeneities. We consider an *inhomogeneous* superconductor consisting of alternating normal and superconducting layers, in the presence of a parallel field. Among artificially layered superconductors, such superlattices have been extensively studied.[7,8] These superconductors are particularly interesting because the strong vortex pinning by the normal-metal layers allows for high critical currents.[9,10] The considered superconductor–normal-metal superlattice can serve as a model of a HTS with periodic distribution of microdefects, modeled by normal layers with proximity-induced superconductivity.[9] From this, we assume that, within the superconducting layers, the Ginzburg-Landau (GL) κ_S parameter is much larger than 1, and $\xi_S(0)$ (the coherence length at $T=0$) is comparable to the crystal lattice constant. The thickness of the normal layers, a_N, is small compared to the superconducting penetration depth λ_S. The coherence length in the normal layers is temperature dependence, but we assume that its characteristic value $\xi_N(T_c)$ is comparable to ξ_S. The above assumptions allow one to obtain an approximate analytical solution for the local magnetic field distribution of the vortex lattice, similar to that of an isolated vortex.[9] The first critical field of the superlattice results from the field penetration in the normal layers. It is smaller than that of the superconductor $(H_{c1}^N<H_{c1}^S)$. In low fields, $H_{c1}^N<H<H_{c1}^S$, stable configurations are commensurate lattices with chains of vortices in the normal layers.[9–11] For $H>H_{c1}^S$, the range of stability of commensurate configurations de-

pends on the pinning strength and on the superlattice period a/λ_S, which determines the geometric commensurability condition for the isotropic vortex lattice.[12] As in Refs. 1 and 2, only the first-order commensurabilities C_n are considered; all vortices are assumed to be within normal regions, with the distance na between the chains of vortices, where n is an integer. However, in the present work the distance between chains is not *a priori* fixed, as distinct from Refs. 1 and 2: the vortex system can choose the equilibrium C_n configuration. Both equilibrium and nonequilibrium initial lattices of isocell triangles can undergo a shear deformation. The pinning strength can be varied, by changing the temperature and the characteristic parameters of the superconducting and normal metals.

In Sec. II, the expressions for free and Gibbs energies of a system of vortices are derived from the GL equations for superconducting and normal metals, assuming that vortices, which occupy every nth layer, can move only within the layers. In Sec. III, the stability of various C_n configurations is analyzed, for two examples of (relatively strong) pinning. In contrast to the results of Refs. 1 and 2, our main result is that for finite pinning strength the equilibrium vortex arrangement is always an isocell triangle lattice, the shear instabilities corresponding to nonequilibrium configurations only.

II. FLUX PENETRATION AND ENERGIES OF VORTEX LATTICES

The shear instabilities of strongly pinned vortex lattices are expected, as stated in the Introduction, in the domain of low fields. At very low fields the superconductor–normal-metal superlattice exhibits a Meissner state, due to the proximity effect from the superconductor. When the magnetic field is larger than the lower critical field H_{c1}^N, vortices form in the superlattice, arranged as chains centered in the normal layers,[9–11] and the vortex lattice is commensurate with the superlattice period. For $H_{c1}^N < H < H_{c1}^S$, candidates for the ground state are the first-order commensurate (C_n) lattices. In the C_n commensurate vortex lattice, chains of vortices in the normal layers are separated by $n-1$ superlattice periods. For $H > H_{c1}^S$, the ground state will be one of the above C_n configurations if H is in the vicinity of one of the matching fields H_M, at which the hexagonal lattice is commensurate with the superlattice.[12] The width of each of these stability domains increases with the pinning potential amplitude. In the case of strong pinning, these domains overlap, and as a result, the ground state can jump from one C_n configuration to the next one. Therefore, considering only the C_n configurations, we evaluate first the local magnetic field distribution and the expressions for free and Gibbs energy of the vortex system from the GL theory. The direction of the external field is chosen as the z axis, and the x axis is perpendicular to the layers. The periodicity of the vortex lattice along the x direction is na. The distance between vortices in each chain, along the y axis, is L_n, and vortices in neighboring rows can be shifted[1,2] by αL_n, where $0<\alpha<1$ (Fig. 1). In the general case, the basis lattice vectors are

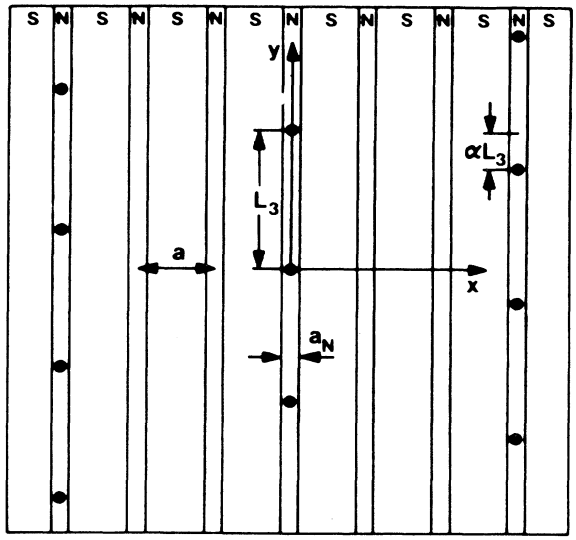

FIG. 1. Commensurate vortex lattice C_n with rows of vortices centered in each nth N layer. The example $n=3$ is presented.

$$\mathbf{r}_{i,j} = ina\,\mathbf{e}_x + (j - i\alpha)L_n\mathbf{e}_y \ , \tag{1}$$

$\alpha=\frac{1}{2}$ corresponding to the initial isocell-triangle lattice without shear.

Since we are interested in the limit

$$\kappa_S \gg 1, \quad \xi_N(T_c) \sim \xi_S(0), \quad a_N \ll \lambda_S(0) \ , \tag{2}$$

we use the London approximation of the GL theory for superconducting and normal metals, valid for large GL parameters.[13] The magnetic energy (per unit area) of the system of vortices, which comes from the local magnetic field and the supercurrents, is given by[9]

$$E = \frac{1}{8\pi A}\int_S [h^2 + \lambda^2(\nabla\times\mathbf{h})^2]d^2\mathbf{r} \ . \tag{3}$$

Here, A is the area occupied by the vortices, $h(\mathbf{r})$ is the local magnetic field, $\lambda^2=\lambda_S^2/g^2$, and g is the normalized order parameter, periodic with period a. In low fields, one can approximate g by the zero-field solution of the GL equations, $g(x)$. Note that the spatial dependence of the magnetic penetration depth $\lambda(x)$ is an important characteristic of superconductor–normal-metal multilayers in a parallel magnetic field.[13] Due to the induced superconductivity, the field screening in normal layers is most effective near superconductor–normal-metal interfaces, where the order parameter $g(x)$ is the greatest, $g(x)\sim 1$. In this region $\lambda(x)$ can be close to λ_S, the penetration depth of a bulk superconductor. In the middle of normal-metal layers, where $g(x)$ is the smallest, $\lambda(x)$ can be much larger.

When the normal layers are much thinner than the superconducting layers, $g(x)$ can be constructed by periodic repetition of the solution obtained in Ref. 9 for a single superconductor–normal-metal–superconductor junction.

The latter is different from 1 only in a small interval that encloses the normal layer and regions of order ξ_S in the superconductor on each side of it,[9]

$$g(x)=\begin{cases}\tanh\left[\dfrac{\beta}{\sqrt{2}\xi_s}\right]\dfrac{\cosh(x/\xi_N)}{\cosh(a_N/\xi_N)}, & |x|<a_N,\\ \tanh\left[\dfrac{|x|+\beta-a_N}{\sqrt{2}\xi_S}\right], & |x|\geq a_N.\end{cases} \tag{4}$$

The constant β is determined from the boundary conditions at the superconductor–normal-metal interfaces,[9]

$$\beta=\frac{\xi_S}{\sqrt{2}}\sinh^{-1}\left[\frac{\sqrt{2}\xi_N}{\xi_S}\coth\left[\frac{a_N}{\xi_N}\right]\right]. \tag{5}$$

In the following, we express all the physical quantities in standard reduced units, relative to the superconductor, taking λ_S as the unit of length, $\sqrt{2}H_c^S$ as the unit of the magnetic field strength, and $(H_c^S)^2/4\pi$ as the unit of energy density. In reduced units, the magnetic energy density $\tilde{E}$ is given by

$$\tilde{E}=\frac{1}{A}\int\left[h^2+\frac{1}{g^2}(\nabla\times\mathbf{h})^2\right]d^2\mathbf{r}\ , \tag{6}$$

where $h(\mathbf{r})$ is the solution of the generalized London equation

$$h-\nabla\frac{1}{g^2}\nabla h=\frac{2\pi}{\kappa_S}\sum_{i,j}\delta(\mathbf{r}-\mathbf{r}_{ij})\ . \tag{7}$$

For $g(x)=1$, this equation reduces to the usual London equation for a homogeneous superconductor;[14] $h(\mathbf{r})$ corresponds to the superposition of fields of individual vortices situated at $\mathbf{r}_{i,j}$. Using Eq. (7), Eq. (3) can be transformed to

$$E=\frac{\kappa_S\tilde{E}}{4\pi}=\frac{1}{2A}\sum_{i,j}h(\mathbf{r}_{ij})=\frac{N_v h(0)}{2A}\ , \tag{8}$$

where $h(0)$ is the magnetic field in the place of the vortex at the (arbitrarily chosen) origin (0,0), generated by the entire vortex lattice, and N_v is the number of vortices on A. In the limit (2), an approximate solution for $h(\mathbf{r})$ in the superconductor–normal-metal superlattice can be obtained from Eq. (7) using methods similar to those for an isolated vortex in a single junction (see Appendix A).

First, from the solution of the magnetic field equation [Eq. (A13)], we calculate the magnetic energy density of the main commensurate configuration C_1,

$$E_1=\frac{\pi}{aL_1^2\kappa_S}\sum_{l=-\infty}^{+\infty}\frac{1}{\Gamma(Q_l^2-1)+2Q_l[\cosh(Q_l a)-\cos(2\pi l\alpha)]/\sinh(Q_l a)}, \tag{9}$$

where $Q_l^2=1+(2\pi/L_1)^2l^2$, and the parameter Γ, given by Eqs. (A8) and (A9) in Appendix A, measures the electromagnetic pinning strength.

The core energy density E^c can be calculated starting with the core energy (per unit vortex length) of an isolated vortex in a superconductor–normal-metal–superconductor junction.[9] This result can be used provided that $a_N\sim 1/\kappa_S\ll 1$, as assumed before. Using the same reduced units as for the electromagnetic energy, we get for $n=1$

$$E_1^c=\frac{1}{8a\kappa_S L_1}\int_{-\pi/2}^{\pi/2}du\left[g^4(x)X_1(x)\cos u+\frac{3g^2(x)}{4}\cos^3 u\right], \tag{10}$$

where $x=(\sqrt{2}/\kappa_S)\tan u$, $X_1(x)=1$ for $|x|>a_N$, and $X_1(x)=0$ for $|x|<a_N$. Note that here it is assumed[9] that $\kappa_N=0$ and $\xi_v=\sqrt{2}/\kappa_S$. Comparing E_1 and E_1^c, Eqs. (9) and (10), it can be checked that in the present case the core energy contribution can be neglected as compared to the electromagnetic energy. Thus we approximate the Gibbs energy density (expressed in the same units as E) by

$$G_1=E_1-\frac{H}{aL_1}\ . \tag{11}$$

In the general case, where vortices occupy every nth normal layer, the same procedure (Appendix B) gives the following expressions for the magnetic energy and Gibbs energy density, respectively:

$$E_n=\frac{\pi}{naL_n^2\kappa_S}\sum_{l=-\infty}^{+\infty}\frac{p_{n,l}}{q_{n,l}}, \tag{12}$$

where

$$p_{n,l}=1+\sum_{i=1}^{n-1}\frac{\Gamma^i(Q_{n,l}^2-1)^i}{Q_{n,l}^i}\frac{[\sinh(Q_{n,l}a)]^{i+1}\cosh[(Q_{n,l}a)]^{n-i-1}}{\sinh(nQ_{n,l}a)},$$

$$q_{n,l}=n\Gamma(Q_{n,l}^2-1)+2Q_{n,l}\frac{\cosh(nQ_{n,l}a)-\cos(2\pi l\alpha)}{\sinh(nQ_{n,l}a)}+\sum_{i=1}^{n-1}\frac{[\Gamma(Q_{n,l}^2-1)\sinh(Q_{n,l}a)]^{i+1}[\cosh(Q_{n,l}a)]^{n-i-1}}{Q_{n,l}^i\sinh(nQ_{n,l}a)},$$

$$Q_{n,l}^2=1+(2\pi/L_n)^2l^2,$$

and

$$G_n = E_n - \frac{H}{naL_n} \ . \tag{13}$$

Here the core energy density

$$E_n^c = \frac{E_1^c}{n} \tag{14}$$

has been neglected for the same reason as above.

The Gibbs energy density is calculated with respect to the Meissner state, and lower critical field of the superlattice (in principle different from that for the superconductor–normal-metal–superconductor junction[9]) is obtained from $G_n(H_{c1}^N)=0$ for $n \gg 1$ and $L_n \gg 1$. From Eqs. (12) and (13), we determine the stable vortex arrangement in equilibrium with the external field, corresponding to the absolute minimum of the Gibbs energy, and calculate the energies of various other vortex configurations, metastable (corresponding to local minima) or unstable.

III. RESULTS AND DISCUSSION

First of all, it is important to find, for a given value of the external field H and of reduced temperature $t=T/T_c$, the ground state for the vortex lattice without shear, for $\alpha=0.5$. To calculate G_n for various n, we first minimize it with respect to intervortex distance L_n within the rows of the configuration C_n. For $n=1$ and $\Gamma \gg 1$ an analytical result can be obtained,

$$\frac{1}{L_1} = \frac{\kappa_S}{\pi} \tanh\left[\frac{a}{2}\right] H \ , \tag{15}$$

whereas in general $L_n(H,t)$ is obtained numerically. Having determined L_n, we have also obtained the elementary cell area $A_n = naL_n$ and the induction $B_n = 2\pi/(\kappa_S A_n)$. Although we work at fixed H and not at fixed induction, we expect that for $\kappa_S \gg 1$ the cell area and the induction do not vary appreciably when n is varied. Deviations from this kind of behaviour, found in some examples, occur when the energy difference between the ground state, $n=n_{\rm eq}$, and the corresponding $C_{n'}$ lattice is large. This indicates an intrinsic instability of $C_{n'}$, where the pinning is not strong enough to maintain the configuration commensurate with the superlattice.

Putting the obtained values of $L_n(H)$ at fixed t in Eq. (13), we obtain G_n as a function of H for each n. We have performed the calculation for the reduced period $a=0.1\sqrt{1-t}$, the reduced temperature $t=0.6$, $\kappa_S=100$, and several values of pinning strength Γ. For our choice of parameters, and in low fields where the electromagnetic pinning is strong,[9,10] both core pinning energy and the core pinning force,[9] calculated starting from Eq. (10), are about two orders of magnitude smaller than the corresponding electromagnetic ones.

For each value of Γ, we have first determined $n_{\rm eq}$ corresponding to the lowest $G_n(H)$ for $\alpha=0.5$ in a range of fields $H_{c1}^N(t) < H \sim H_{c1}^S(t)$. Next, for a fixed value of the external field within this range, we considered several C_n configurations, allowing shear along the normal layers, and varying α from 0.5 to 1 at fixed A_n.[1] The corresponding free energies $E_n(\alpha)$ are calculated for the same value of Γ and for several n.

We present below two typical examples. For $\Gamma=3.15$, obtained for $a_N/\xi_N(T_c)=6.5$, $G_n(H)$ is plotted for $\alpha=\frac{1}{2}$ in the range $0.0080 < H < 0.0128$ for several values of n ($n=23$, 7, 4, and 3) in Fig. 2. It is seen that $n_{\rm eq}=23$ up to $H=0.0120$. For the same values of Γ and n as in Fig. 2 and for $H=0.0096$, $E_n(\alpha)$ dependencies are given in Fig. 3. Energies as functions of α for both $n=23$ and $n=7$ exhibit a single minimum, but in the latter case $\alpha \neq 0.5$. For $n=4$ there are two minima, whereas for $n=3$ the energy has a set of local minima and maxima. The comparison of Gibbs energies $G_n(\alpha_{\rm min})$ at $H=0.0096$ shows that in the equilibrium configuration n is again equal to $n_{\rm eq}=23$ and $\alpha=0.5$. The lattices obtained by shear deformation have higher energy. The maximum relative energy difference between the above configurations is $|(G_{23}-G_3)/G_{23}| \sim 0.1$.

For stronger pinning, $\Gamma=24.32$, obtained for $a_N/\xi_N(T_c)=9.2$, in the same range of extermal fields the ground state without shear is found to be $n_{\rm eq}=8$. [We do not present here the $G_n(H)$ dependencies, since they are similar to those in Fig. 2.] The characteristic $E_n(\alpha)$ dependencies, with one unshifted and one shifted minimum and two minima, are obtained at $H=0.0096$ for $n=8$, 4, and 2, respectively. A set of local minima, lying between the maxima which are at the values of α corresponding to the rational numbers (Farey numbers[1]), is found for $n=1$ (Fig. 4). The most stable configuration for any α is again that with $n=8$, $\alpha=0.5$. The relative energy difference $|(G_8-G_1)/G_8| \sim 0.02$ is comparable to the energy difference between the square and triangular lattices in the isotropic case.

In all analyzed cases, the equilibrium configurations $n=n_{\rm eq}$ are found to be those with $\alpha=0.5$. For larger Γ, $n_{\rm eq}$ is smaller, since the stronger pinning is capable of maintaining a commensurate lattice with closer rows. When α is varied so that the system of vortices is passing through a set of different lattices, the function $E_n(\alpha)$ exhibits one or more minima and maxima. When n is far enough from $n_{\rm eq}$, a complex structure of extrema is obtained [Figs. 3(d) and 4].

To obtain the general condition for appearance of a set of extrema, we rewrite Eq. (9) in the form

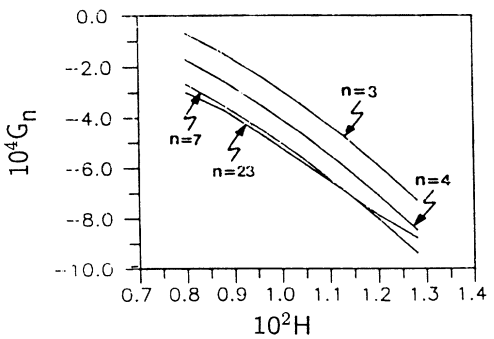

FIG. 2. Gibbs energy density G_n vs external magnetic field H (in reduced units) for several C_n configurations, $n=23$, 7, 4, and 3, and for $\Gamma=3.15$.

$$E_1=\frac{4\pi}{\kappa_S L_1^2}\sum_{l=-\infty}^{\infty}\frac{\sin^2(\pi l\alpha)}{[\Gamma(Q_{1,l}^2-1)(\sinh Q_{1,l}a)/4Q_{1,l}+\sinh^2(Q_{1,l}a/2)+\sin^2(\pi\alpha l)]}\frac{\coth(Q_{1,l}a/2)}{Q_{1,l}a/2}f_l(\Gamma)\ , \tag{16}$$

where

$$f_l(\Gamma)=\frac{1}{1+\dfrac{\Gamma(Q_{1,l}^2-1)\coth(Q_{1,l}a/2)}{2Q_{1,l}}}\ .$$

The necessary condition for pronounced extrema is, similarly to Ref. 1, that the two first two terms in the square bracket in the denominator should be comparable to the last one, i.e., $x_1=a\pi/L_1\ll 1$. A similar condition can be derived in the case when every nth layer is occupied by vortices:

$$x_n=\frac{na\pi}{L_n}\ll 1\ . \tag{17}$$

Note that the strongest influence of the pinning strength enters via $L_n(\Gamma)$. From the above criterion, and in accordance with our numerical results, we see that a complex structure of $E_n(\alpha)$ corresponds to small n, i.e., to lattices which are not stable in low fields. To investigate if this correspondence holds in the general case, we perform the following calculations. As in Refs. 1 and 2, we fix n, and we vary the external field, assuming that the vortex lattice is in the C_n configuration. Assume that at some relatively high field a given C_n configuration with $\alpha_{\min}=\frac{1}{2}$ is the equilibrium configuration. If the field strength is reduced, a set of new ground states appears. As a result, C_n becomes more and more unstable. At the same time, the minimum of the $E_n(\alpha)$ curves shifts from $\alpha=\frac{1}{2}$, and a set of extrema develops. This is illustrated, for pinning strength $\Gamma=3.15$, on the example of the C_3 lattice, which is expected to be stable in fields much higher than $H_{c1}^S=\ln\kappa_S/2\kappa_S=0.023$. We investigated the range of fields from $H=0.080$ (where C_3 is not stable, but $\alpha_{\min}=\frac{1}{2}$) to $H=0.0072$. Two typical results are presented in Fig. 5. At $H=0.040$, the minimum of $E_3(\alpha)$ is shifted to $\alpha=0.6$ and the set of extrema which is seen at $H=0.0096$ [Fig. 3(d)] is even more developed at $H=0.0076$ and in lower fields. For H below 0.0076, the vortex distance L_3 becomes unrealistically large, the Gibbs energy relative difference between the C_3 configurations at $H=0.0040$ and $H=0.0076$ being of the order of unity. As in Ref. 1, the plot of the positions of all minima of the free energy as a function of $x_3=3\alpha\pi/L_3$ (Fig. 6) has a hierarchial structure. (Note that in our case x_n is proportional to the magnetic induction B_n, decreasing with decreasing field H; it is directly proportional to H only in the strong-pinning limit, $\Gamma\gg 1$.) At relatively high field, i.e., at large x_3, there is a single minimum for $\alpha=0.5$ corresponding to an isocell lattice. With decreasing field, a bifurcation occurs for $x_3=0.12$. Further decrease of H induces the appearance

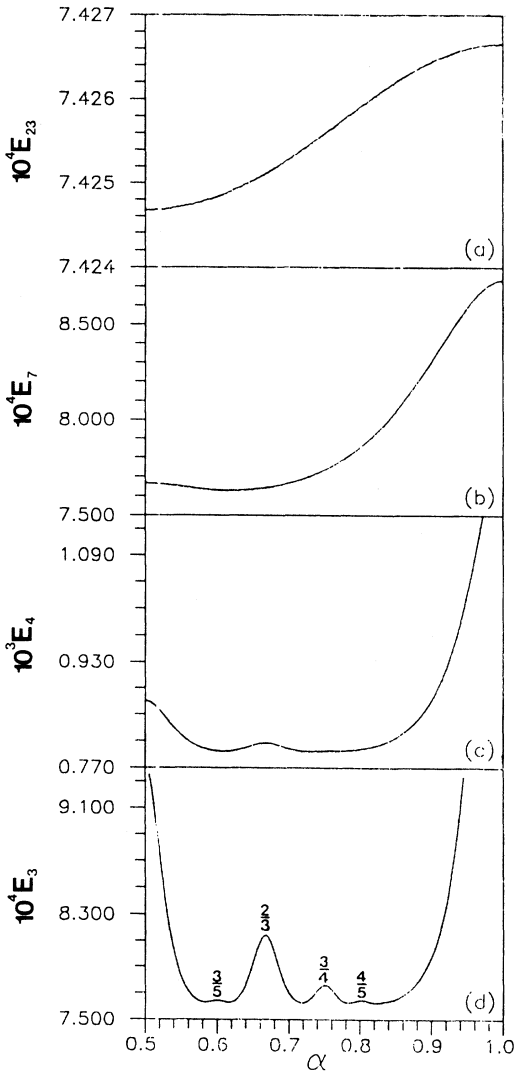

FIG. 3. Free-energy desity E_n as a function of the shear parameter $0.5<\alpha<1$ for $\Gamma=3.15$ and $H=0.0096$. (a) $n=23$, (b) $n=7$, (c) $n=4$, and (d) $n=3$.

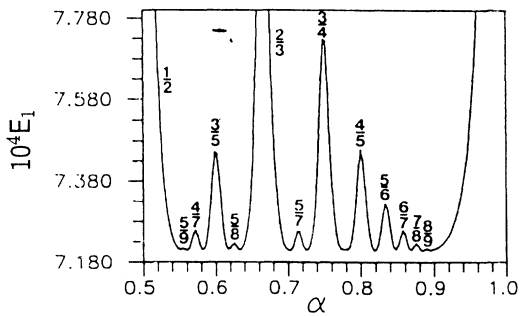

FIG. 4. Free-energy density E_n as a function of α for $\Gamma=24.32$, $H=0.0096$, and $n=1$.

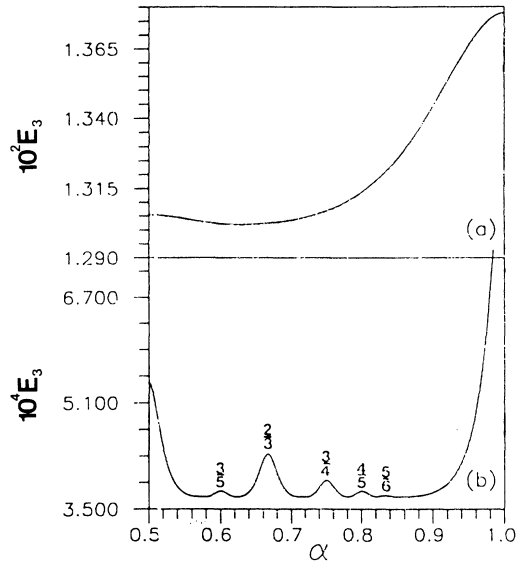

FIG. 5. Qualitative change in the free-energy variation $E_n(\alpha)$ with decreasing field H, illustrated for $n=3$ and $\Gamma=3.15$ on the examples (a) $H=0.040$ and (b) $H=0.0076$.

of quasibifurcations at every minimum of the function $E_3(\alpha)$. There is only one unbroken trajectory of $\alpha_{\min}$, starting at $\alpha=0.5$ and, with decreasing $x_3(H)$, tending to the value $\alpha=\tau=(\sqrt{5}-1)/2\approx 0.618$, which is the golden mean. This is the trajectory of the absolute minima of $E_3(\alpha,H)$.

The bifurcation diagram is very similar to (x,α) diagrams obtained for vortex lattices from anisotropic London theory,[1,2] and in numerical simulations of the growth of spiral structures.[3,4] In the first case,[1] x is proportional to H, and α has the same meaning as here. In the second case, x corresponds to the parameter G of the quantized logarithmic spiral[15] $r_N=r_0e^{NG}$, $\theta_N=N\phi_d$, where N is an integer and α corresponds to the divergence angle ϕ_d.[3] For vortex lattices on analogy with spiral arrangements can be seen with the help of Eq. (1). The shear deformations are related to the displacements along the layers, and

$$\frac{|y_{N,j}-y_{0,j}|}{L_n}=N\alpha \quad \forall\ (j,n) \tag{18}$$

corresponds to

$$r_N/r_0=\theta_N=N\alpha\ , \tag{19}$$

which is the equation of the Archimedian spiral.[15] The continuous transition from one spiral arrangement (with $\alpha=\frac{1}{2}$) to another (with α being the ratio of two consecutive members in the Fibonacci series) is obtained, as in simulations,[4] by the continuous decrease of the control parameter x_n, i.e., of the induction B_n. This change occurs by adding or removing an integer number of flux quanta (vortices). As in spiral growth, the new arrangement, found from the requirement of lowest energy, is such that the system selects the divergence angles converging towards the simplest irrational numbers. The physical origin of this selection is in the repulsive interactions between the elements in search of minimum energy deposition. An important point is that the quasibifurcations occur at small x_n. In the anisotropic model,[1,2] where n is fixed, and the anisotropy parameter is $\epsilon=\sqrt{m_\perp/m_\parallel}$, the control parameter x is, in our notation, $x_n=\epsilon n a\pi/L_n$. To achieve small x_n for strong anisotropy, implicit in the strong-pinning assumption,[1,2] this requires very low fields. In our inhomogeneous model, smaller x_n (for n fixed) means also lower field, i.e., transitions to more and more energetically unstable structures.

The main difference between our and previous works[1,2] is that in the latter case the shear instability is *always* induced in low fields, where one finds[2] that in addition to the ground state there are also several metastable states, whose number grows for decreasing field. In our approach, were the finite pinning strength Γ enters explicitly into the calculation, and the vortex system is allowed to select the equilibrium configuration, we find that $n_{\rm eq}(H)$ depends on the Γ, but $\alpha_{\rm eq}=0.5$ in all analyzed cases: the ground-state vortex arrangement is a lattice of isocell triangles, without shear. Complex structures of $E_n(\alpha)$ curves correspond to sets of states with higher energies. However, with increasing Γ the energy difference between various C_n configurations diminishes and it is possible that the nonequilibrium C_n configurations, forming a glassy state, are created during a rapid decrease of the magnetic field, new vortices not having time to occupy optimal positions.[2] With our inhomogeneous model, we are able to calculate the energy of such configurations and to estimate the probability of the glassy states.

In conclusion this work provides a theoretical criterion for the appearance of sheared commensurate vortex configurations in low fields. In physical measurements, we expect nonsheared isocell-triangle lattices to be observed as the equilibrium states. This should be possible (by neutron diffraction[16] or, indirectly, by the muon-spin

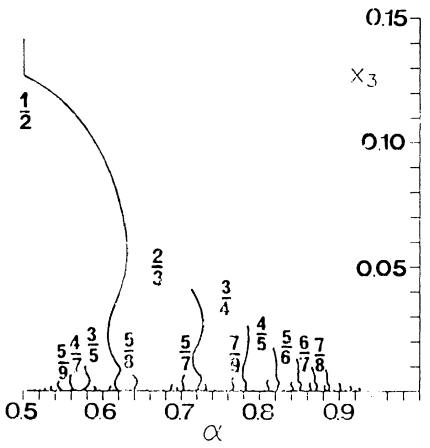

FIG. 6. Positions $\alpha_{\min}$ of the minima of $E_3(\alpha)$ curve as functions of x_3, for $\Gamma=3.15$.

rotation technique[17]) in artificially prepared layered superconductors, with a low concentration of random pinning centers. If under nonequilibrium conditions the sheared lattices or the corresponding vortex glass are observed, this would be a clear signature of extremely strong pinning, since only in this limit do the sheared lattices become energetically concurrent.

ACKNOWLEDGMENTS

We thank Z. Radović for helpful discussions.

APPENDIX A

In this Appendix, we calculate the field distribution for the main commensurate configuration (C_1), with vortex chains in every N layer. In this case, $n=1$, the elementary cell area is $A_1=aL_1$ and $A=NaL_1$. To solve Eq. (7), we take the field as periodic along the y direction,

$$h(x,y)=\frac{1}{L_1}\sum_{\forall l} e^{(2\pi i l y/L_1)} h_l(x) . \tag{A1}$$

Then Eq. (7) becomes

$$h_l(x)-\frac{d}{dx}\frac{1}{g^2}\frac{dh_l(x)}{dx}+\frac{1}{g^2}\frac{4\pi^2 l^2}{L_1^2}h_l(x) = \frac{2\pi}{\kappa_S}\sum_n \delta(x-na)e^{2\pi i n l\alpha} , \tag{A2}$$

where we have used the Poisson formula to transform the right-hand side. It can be seen that, when $x\to x+a$, one has

$$h_l(x+a)=e^{2\pi i l\alpha}h_l(x) , \tag{A3}$$

which means that it is necessary to solve Eq. (A2) only in the interval $[-a/2,a/2]$. In this region Eq. (A2) becomes

$$Q_{1,l}^2 h_l(x)-\frac{d}{dx}\frac{1}{g^2}\frac{dh_l(x)}{dx} +\frac{4\pi^2 l^2}{L_1^2}\left[\frac{1}{g^2}-1\right]h_l(x)=\frac{2\pi}{\kappa_S}\delta(x) , \tag{A4}$$

where $Q_{1,l}^2=1+(4\pi^2 l^2/L_1^2)$. Equation (A4) describes the influence of the N layers on field distribution in regions (denoted by M) where $g(x)\neq 1$. Outside of M, which is of a reduced thickness of order $1/\kappa_S$, this equation can be approximated by the homogeneous equation

$$Q_{1,l}^2\tilde{h}_l-\tilde{h}_l''=0 , \tag{A5}$$

where $\tilde{h}_l$ is the approximate solution of Eq. (A4), which is asymptotically equal to h_l outside M. The solution of Eq. (A5) is then

$$\tilde{h}_l(x)=\begin{cases} A_l\cosh(Q_{1,l}x)+B_l\sinh(Q_{1,l}x) & \text{for } -\frac{a}{2}<x<0, \\ C_l\cosh(Q_{1,l}x)+D_l\sinh(Q_{1,l}x) & \text{for } 0<x<\frac{a}{2}. \end{cases} \tag{A6}$$

The coefficients A_l, B_l, C_l, and D_l can be determined from the boundray conditions at the N layer, and the periodicity requirements, using Eq. (A3). Following Ref. 9, we integrate Eq. (A2) in the interval $(-M/2,M/2)$ to obtain the boundary condition for the derivative of $\tilde{h}_l(x)$. Since at the end of this interval h_l is asymptotically equal to the solution $\tilde{h}_l(x)$, and $h_l(0)=\tilde{h}_l(0)$, with accuracy $h_l(0)/\kappa_S$ when $a_N\sim 1/\kappa_S$, we get

$$-\frac{d\tilde{h}_l(x)}{dx}\Bigg|_{-0}^{+0}+\frac{4\pi^2 l^2}{L_1^2}\Gamma\tilde{h}_l(0)=\frac{2\pi}{\kappa_S} , \tag{A7}$$

where

$$\Gamma=\int dx\,[g(x)^{-2}-1] , \tag{A8}$$

or explicitly

$$\Gamma=2\sqrt{2}\left[\coth\left[\frac{\beta\kappa_S}{\sqrt{2}}\right]-1\right]\frac{1}{\kappa_s} +\xi_N\sinh\left[\frac{a_N}{\xi_N}\right]\coth^2\left[\frac{\beta\kappa_S}{\sqrt{2}}\right]-a_N . \tag{A9}$$

The next boundary condition follows from symmetry by replacing x with $-x$,

$$\tilde{h}_l(-0)=\tilde{h}_l(+0) , \tag{A10}$$

and from Eq. (A3) we get

$$\tilde{h}_l\left[-\frac{a}{2}\right]=e^{2\pi i l\alpha}\tilde{h}_l\left[\frac{a}{2}\right] \tag{A11}$$

and

$$\tilde{h}_l'\left[-\frac{a}{2}\right]=e^{2\pi i l\alpha}\tilde{h}_l'\left[\frac{a}{2}\right] . \tag{A12}$$

The solution of Eq. (A5) satisfying Eqs. (A7), (A10), (A11), and (A12) is

$$\tilde{h}_l(x)=\frac{2\pi}{\kappa_S}\left\{\frac{\cosh(Q_{1,l}x)}{\Gamma(Q_{1,l}^2-1)+2Q_{1,l}[\cosh(Q_{1,l}a)-\cos(2\pi l\alpha)]/\sinh(Q_{1,l}a)}\right.$$
$$\left.+\frac{[\cosh(Q_{1,l}a)-\cos(2\pi\alpha l)]\sinh(Q_{1,l}x)}{\Gamma(Q_{1,l}^2-1)+2Q_{1,l}[\cosh(Q_{1,l}a)-\cos(2\pi l\alpha)]/\sinh(Q_{1,l}a)}\right\}, \tag{A13a}$$

for $-a/2<x<0$, and for $0<x<a/2$

$$\tilde{h}_l(x)=\frac{2\pi}{\kappa_S}\left\{\frac{\cosh(Q_{1,l}x)}{\Gamma(Q_{1,l}^2-1)+2Q_{1,l}[\cosh(Q_{1,l}a)-\cos(2\pi l\alpha)]/\sinh(Q_{1,l}a)}\right.$$
$$\left.-\frac{[\cosh(Q_{1,l}a)-\cos(2\pi\alpha l)]\sinh(Q_{1,l}x)}{\Gamma(Q_{1,l}^2-1)+2Q_{1,l}[\cosh(Q_{1,l}a)-\cos(2\pi l\alpha)]/\sinh(Q_{1,l}a)}\right\}. \tag{A13b}$$

APPENDIX B

To calculate the field distribution for the nth commensurate configuration (C_n), we start with $n=2$. In this case, it is necessary to solve Eq. (A5) only in the interval $2a$, e.g., $(-a/2,3a/2)$. In this region, the boundary conditions are

$$-\frac{d\tilde{h}_l(x)}{dx}\Bigg|_{-0}^{+0}+\frac{4\pi^2l^2}{L_2^2}\Gamma\tilde{h}_l(0)=-\frac{2\pi}{\kappa_S}\ , \tag{B1a}$$

$$\tilde{h}_l(-0)=\tilde{h}_l(+0), \tag{B1b}$$

$$-\frac{d\tilde{h}_l(x)}{dx}\Bigg|_{a-0}^{a+0}+\frac{4\pi^2l^2}{L_2^2}\Gamma\tilde{h}_l(a)=0\ , \tag{B1c}$$

$$\tilde{h}_l(a-0)=\tilde{h}_l(a+0)\ , \tag{B1d}$$

$$\tilde{h}_l\left[-\frac{a}{2}\right]=e^{2\pi il\alpha}\tilde{h}_l\left[\frac{3a}{2}\right]\ , \tag{B1e}$$

and

$$\tilde{h}_l'\left[-\frac{a}{2}\right]=e^{2\pi il\alpha}\tilde{h}_l'\left[\frac{3a}{2}\right]\ . \tag{B1f}$$

For $n>2$ the similar procedure can be done in the interval na. It was performed explicitly for $n=3$ and 4, and by induction the result for any $n\geq 1$ [Eq. (12)] was derived.

[1] L. S. Levitov, Phys. Rev. Lett. **66**, 224 (1991).
[2] B. I. Ivlev, N. B. Kopnin, and V. L. Pokrovsky, J. Low Temp. Phys. **80**, 187 (1990).
[3] S. Douady and Y. Couder, La Recherche **24**, 26 (1993).
[4] S. Douady and Y. Couder, Phys. Rev. Lett. **68**, 2098 (1992).
[5] M. Tachiki and S. Takahashi, Solid State Commun. **70**, 291 (1989).
[6] V. G. Kogan and L. J. Campbell, Phys. Rev. Lett. **62**, 1552 (1989).
[7] B. Y. Jin and J. B. Ketterson, Adv. Phys. **38**, 189 (1989).
[8] I. K. Schuller, J. Guimpel, and Y. Bruynseraede, Mater. Res. Bull. **15**, 29 (1990).
[9] D. Davidović and L. Dobrosavljević-Grujić, Phys. Rev. B **43**, 2809 (1991).
[10] L. Dobrosavlejević-Grujić, V. Prokić, and D. Davidović, in *Proceedings of SPIE OE/LASE '94, Superconducting Superlattices and Multilayers,* edited by I. Božovic, SPIE Proc. 2157 (SPIE, Bellingham, WA, 1994), p. 50; Phys. Rev. B (to be published).
[11] L. Dobrosavljević and P. G. de Gennes, Solid State Commun. **5**, 177 (1967).
[12] S. Ami and K. Maki, Prog. Theor. Phys. **53**, 1 (1975).
[13] For GL theory of the superconductor–normal-metal proximity system and its London limit, see Refs. 9–11 and references therein.
[14] P. G. de Gennes, *Superconductivity* (Benjamin, New York, 1966).
[15] L. A. Bursill, Peng Ju Lin, and Fan Xudong, Mod. Phys. Lett. **1**, 195 (1987).
[16] P. Gammel, D. A. Huse, R. N. Kleiman, B. Batlogg, C. S. Oglesby, E. Bucher, D. J. Bishop, T. E. Mason, and K. Mortensen, Phys. Rev. Lett. **72**, 278 (1994).
[17] E. H. Brandt, J. Low Temp. Phys. **73**, 355 (1988); R. Cubbit, E. M. Forgan, M. Warden, S. L. Lee, P. Zimmermann, H. Keller, I. M. Savić, P. Wenk, D. Zech, P. H. Kes, T. W. Li, A. A. Mekovsky, and Z. Tarnawski, Physica C **213**, 126 (1993); F. N. Gygax, B. Hitti, E. Lippelt, A. Schenck, D. Cattani, J. Cors, M. Decroux, O. Fischer, and S. Barth, Europhys. Lett. **4**, 473 (1987).